

Hierarchical Porous Carbon Microspheres Derived from Biomass-Corncob as Ultra-High Performance Supercapacitor Electrode

Lili Wang¹, Yanting Li¹, Kunlong Yang¹, Wenqi Lu¹, Jianguo Yu¹, Jian Gao¹, Gang Liao¹, Yuning Qu^{1,*}, Xiaofeng Wang², Xifei Li³, Zhen Yin^{1,*}

¹ State Key Laboratory of Separation Membranes and Membrane Processes, School of Environment and Chemical Engineering, Tianjin Polytechnic University, 399 Binshui West Road, Tianjin 300387, P. R. China

² State Key Laboratory of Inorganic Synthesis and Preparative Chemistry, College of Chemistry, Jilin University, Changchun 130012, P. R. China

³ Tianjin International Joint Research Centre of Surface Technology for Energy Storage Materials, College of Physics and Materials Science, Tianjin Normal University, Tianjin 300387, P. R. China

*E-mail: qu_yuning0323@163.com, yinzhen@tjpu.edu.cn

Received: 9 March 2017 / Accepted: 28 March 2017 / Published: 12 May 2017

The hierarchical porous carbon microspheres (HPCS) were obtained using corn cob as precursor via a facile and cost-effective approach. The porous carbon microspheres exhibited regular spherical morphology, hierarchical porous, localized graphitization structure and the oxygen-containing functional groups on the surface of carbon spheres. The pore size and specific surface area could be tuned by the amount of KOH during the activation process. The porous carbon microspheres displayed maximum specific capacitance of 384.5 F/g at scan rate of 5 mV/s and ultra-high rate capacitance of 137.3 F/g at the current density of 100 A/g. The high capacitance retention of the porous carbon microspheres (over 97%, even with 5000 charge/discharge cycles) demonstrated its superior cycling stability. Moreover, high power density (62.9 kW/kg) and energy density (33.4 Wh/kg) could be achieved at 120 A/g. Hence, the ultrahigh specific capacitance and exceptional cyclic stability of the porous carbon microspheres indicate its significant potential application in the field of energy storage.

Keywords: Biomass, Carbon microspheres, Hierarchical pore, Supercapacitors

1. INTRODUCTION

During past decades, traditional energy production leads to the energy crisis, increasing global climate warming and severe environmental pollution due to the combustion of non-renewable fossil

fuels. Energy supply and environmental pollution have become two of the most significant challenges for sustainable development, especially for rapidly developing economies. In order to address these issues, the researchers have been striving to exploit clean and renewable resources, such as fuel cells [1,2] and solar cells, as well as developing environmentally-friendly, low-cost and advanced energy storage devices [3]. Most recently, supercapacitors have attracted increasing attention as alternative energy-storage systems due to their superior rate performance, high power densities, long-term cycling stability and good safety [4,5]. In general, for the supercapacitors, there have two different types, i.e. electrical double-layer capacitors (EDLCs) and pseudocapacitors. For the EDLCs, it has been widely used in portable electronic devices originating from their suitable pore size and high specific surface area [6,7]. Of course, the key factor of the EDLCs is the electrode materials. Carbon materials, such as graphene, carbon fibers and carbon spheres, are widely utilized as active electrode materials in EDLCs because of their non-toxicity, high chemical stability, high specific surface area and good electronic conductivity [8-10]. Among the above carbon materials, the porous carbon microspheres (PCS) have drawn extensive attention due to their unique properties, which can reduce the resistance of ion diffusion and the package porosity, thus benefiting the formation of ion buffer reservoirs and decrease of the ion diffusion distance [11,12]. Therefore, tremendous efforts have been devoted on the fabrication of PCS with regular geometry or tunable pore structure for high performance EDLCs.

Usually, the hard template strategy can be adopted to prepare PCS. For example, the modified Stöber route has been used to prepare effectively PCS using silica spheres as hard template [13-15]. Moreover, the additional mesopores can be formed due to the packing of small carbon spheres [16]. However, the surface area of porous carbon spheres via traditional template methods was very limited. Hence, it is hard to achieve high specific capacitance based on energy storage mechanism of EDLCs. Therefore, it is of significance to fabricate PCS with hierarchical pore structure and large surface area for electrode materials of ultra-high performance EDLCs. Recently, the chemical activation methods have been reported as efficient way to improve the pore structure, and thus enhance surface area of carbon spheres. Actually, it can involve two stages that the carbon spheres were firstly prepared and then followed by chemical activation at high temperature [11,17,18]. However, the precursor of the carbon spheres are usually pure reagents with high costs, such as glucose, starch, pectin, and benzene [19-20]. Considering requirement of sustainable eco-friendly process or resources, it's greatly desirable to transform biomass to valuable carbon materials. As known to all, biomass is one type of renewable energy, which is rich in hemicellulose, cellulose and lignin. For instance, the annual output of corncob worldwide is about 41-54 million metric tons [21] and the content of hemicellulose and cellulose is higher (about 70%), which has been used for the production of biofuels, varieties of chemicals with high value in large scale, and activated carbons as biosorbent for metal and dye. Obviously, it's a viable renewable source of carbon materials for energy applications [22-24] because they are readily available, regenerate rapidly, low cost and environment friendly compared with the fossil fuels. Although biomass derived porous carbons have been extensively prepared by physical or chemical activation methods [9,25-28], the obtained products usually exhibit irregular morphology and poor electrochemical performances. Hence, it is great challenging to design biomass derived porous carbon microspheres with superior supercapacitive performances.

In the present work, the carbon microspheres were prepared using corncob as carbon precursor via the low-temperature hydrothermal method, followed KOH activation in order to get the hierarchical porous structures. The carbon microspheres with tuned pore size exhibited the unique porous structure, rendering the carbon microspheres excellent supercapacitive properties. The electrochemical results showed the HPCS exhibited superior supercapacitive performance, i.e. high specific capacitance, ultra-high rate performance and outstanding cycling stability. Moreover, the fabricated symmetric supercapacitors with the porous carbon microspheres can also reveal high energy densities and power densities, confirming their potential application as electrode in capacitor device.

2. MATERIALS AND METHODS

2.1. Materials

Corn cob were obtained from a corn mill nearby Tianjin. The corn cob was sieved regular granules with the size of 120-150 μm and then dried at 90 $^{\circ}\text{C}$ overnight. H_2SO_4 and KOH were all of analytical grade.

2.2. Preparation of HPCS

Firstly, the corn cob were hydrolyzed with sulfuric acid (65 wt.%) with the ratio of corn cob mass to the solution volume was 1:10 (g/mL). The hydrolysis reaction was carried out at 55 $^{\circ}\text{C}$ for 10 min. After above reaction, in order to obtain the solution with acid concentrations of 30%, water was added to the hydrolysis solution. After filtration, the filtrate was carbonized at 160 $^{\circ}\text{C}$ for 6 h to get carbon spheres by hydrothermal method. And then, the product were washed with distilled water until neutrality and dried at 110 $^{\circ}\text{C}$ for 12 h. The carbon spheres were pretreated in a tubular furnace at 500 $^{\circ}\text{C}$ for 1 h under nitrogen atmosphere before activation. The pretreated carbon spheres were mixed with KOH in crucible, and the mass ratio of carbon spheres/KOH was 1:3, 1:4 and 1:5, then the mixture were heated up to 400 $^{\circ}\text{C}$ for 0.5 h, and then to 800 $^{\circ}\text{C}$ in furnace with nitrogen atmosphere for 1 h. Finally, the product was washed and dried to get the HPCS. Samples obtained at different mass ratio of carbon spheres/KOH were identified as HPCS-3, HPCS-4, and HPCS-5, respectively.

2.3. Materials characterization

The surface physical morphology were observed with field-emission scanning electron microscopy (FE-SEM), i.e. Hitachi S-4800. The high resolution transmission electron microscopy (HR-TEM) measurement was taken on TECNAI G², FEI. The structure of samples were characterized with the X-ray powder diffraction (XRD), which were tested on a Shimadzu 6000 diffractometer with Cu K α radiation ranging from 10 to 80 $^{\circ}$. The Raman spectra were carried out on the Lab RAM ARAMIS spectrometer. X-ray photoelectron spectroscopy (XPS) spectra were recorded on a Thermo

Fisher Scientific K-Alpha spectrometer. The N₂ adsorption-desorption isotherms were measured on ASAP 2420 Micromeritics instrument.

2.4. Electrochemical Measurement

The preparation of working electrodes was similar to our previous work [30]. Briefly, the mass fraction of HPCS, polytetrafluoroethylene (PTFE, 60 wt%) and acetylene black were 80 wt%, 10 wt% and 10 wt% respectively, and then mixed in ethanol and ultrasonicated. Subsequently, slurry of the mixtures were pressed on the nickel foam. The obtained electrodes were dried at 110 °C for 12 h, and then soaked in 6 M KOH solution for 24 h. Finally, two electrodes were sandwiched into a coin cell (CR2032 type) for the electrochemical tests. The electrochemical tests, including cyclic voltammetry (CV), galvanostatic charge/discharge and electrochemical impedance spectroscopy (EIS) tests were carried out with a Zennium-IM6 electrochemical station. The EIS were conducted with frequency range between 1 Hz and 82.5 kHz, which were analyzed with Nyquist plots. The specific capacitance values (C_s , F/g) were estimated from CV curves by equation (1) [10]:

$$C_s = \frac{4A}{m \times \Delta V \times \nu} \quad (1)$$

where A is the integrating area of CV curves, m (g) represents total mass of the active materials, ΔV and ν are the potential window and scan rate, respectively.

For the two electrode cells, the specific capacitance values can be calculated from galvanostatic charge/discharge (GCD) with the equation (2) [10, 29]:

$$C_s = \frac{4I\Delta t}{m \times \Delta V} \quad (2)$$

Where I is the constant current (A), Δt is the discharge time (S), m is the whole mass (g) of electrode materials and ΔV is the voltage change during the discharge process (V).

The energy density (E) and power density (P) can be calculated from the specific capacitance values (C_s) with the following equations: [30-32]:

$$E = \frac{1}{2} C_s \Delta V^2 \quad (3)$$

$$P = \frac{E}{t} \quad (4)$$

Where C_s is the specific capacitances, t is the discharge time, and ΔV is the voltage change subtracted the IR drop during the discharge process.

3. RESULTS AND DISCUSSION

3.1. Characterisation of the HPCS

The HPCS were designed via a simple hydrothermal method and activation process (Scheme 1). The corncob was degraded into monosaccharides via hydrolysis process and then transformed into

carbon microspheres through hydrothermal carbonization. Finally, the hierarchical porous structures in carbon microspheres were formed after KOH activation process.



Scheme 1. Schematic diagrams illustrate the preparation process of hierarchical porous carbon microspheres.

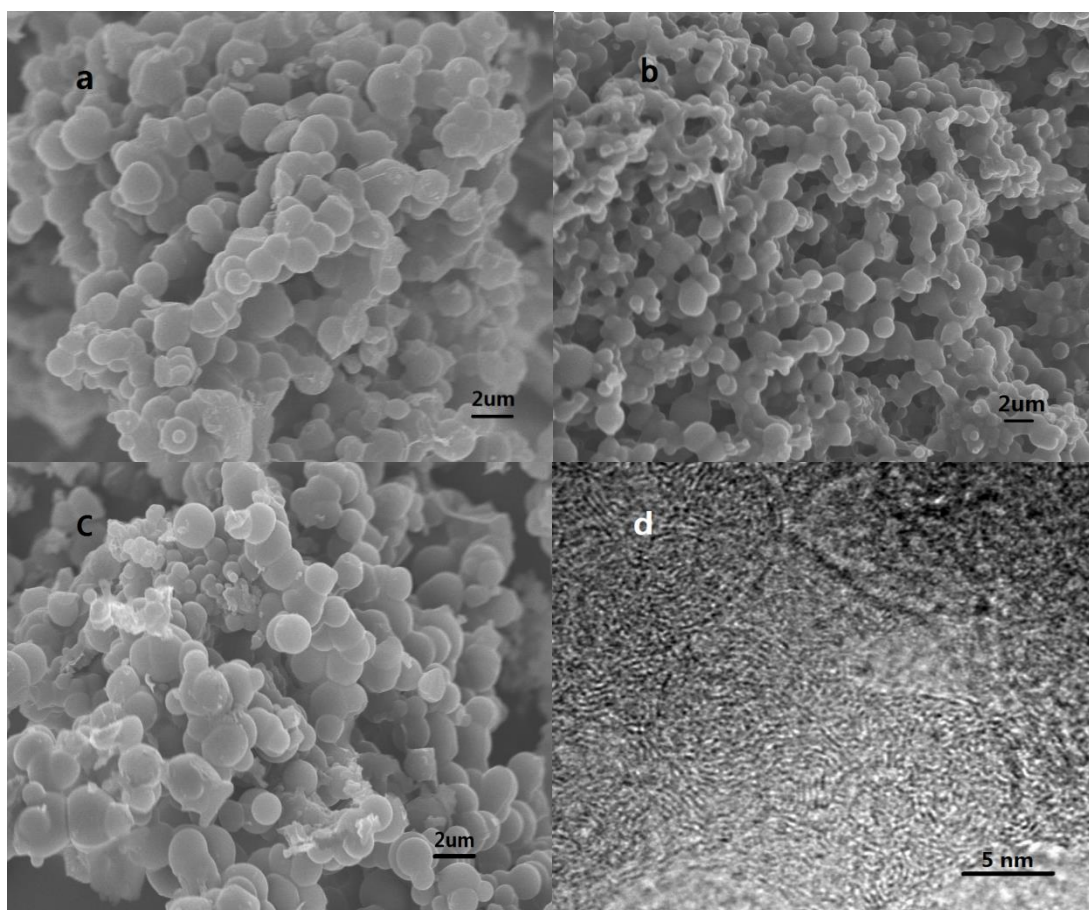


Figure 1. SEM images of (a) HPCS-3, (b) HPCS-4, (c) HPCS-5 and (d) HR-TEM image of HPCS-4.

As shown in Fig. 1a-c, the obtained product after activation with different amount of KOH displayed smooth surface and sphere-like morphology with average size of about 1.5 - 2 μm, indicating that the spherical morphology of the HPCS were not obviously affected by the amount of KOH. The

HR-TEM image of the HPCS-4 (Fig. 1d) confirmed that the carbon spheres had developed pore structure and localized ordered structure of graphite. Obviously, the regular morphology, smooth surface, good liquidity, developed pores and localized graphite structure in carbon microspheres would enhance electrochemical performance of EDLCs due to the package porosity among the carbon spheres, which would reduce the resistance and distance of ion diffusion, facilitate the generation of ion buffer reservoirs.

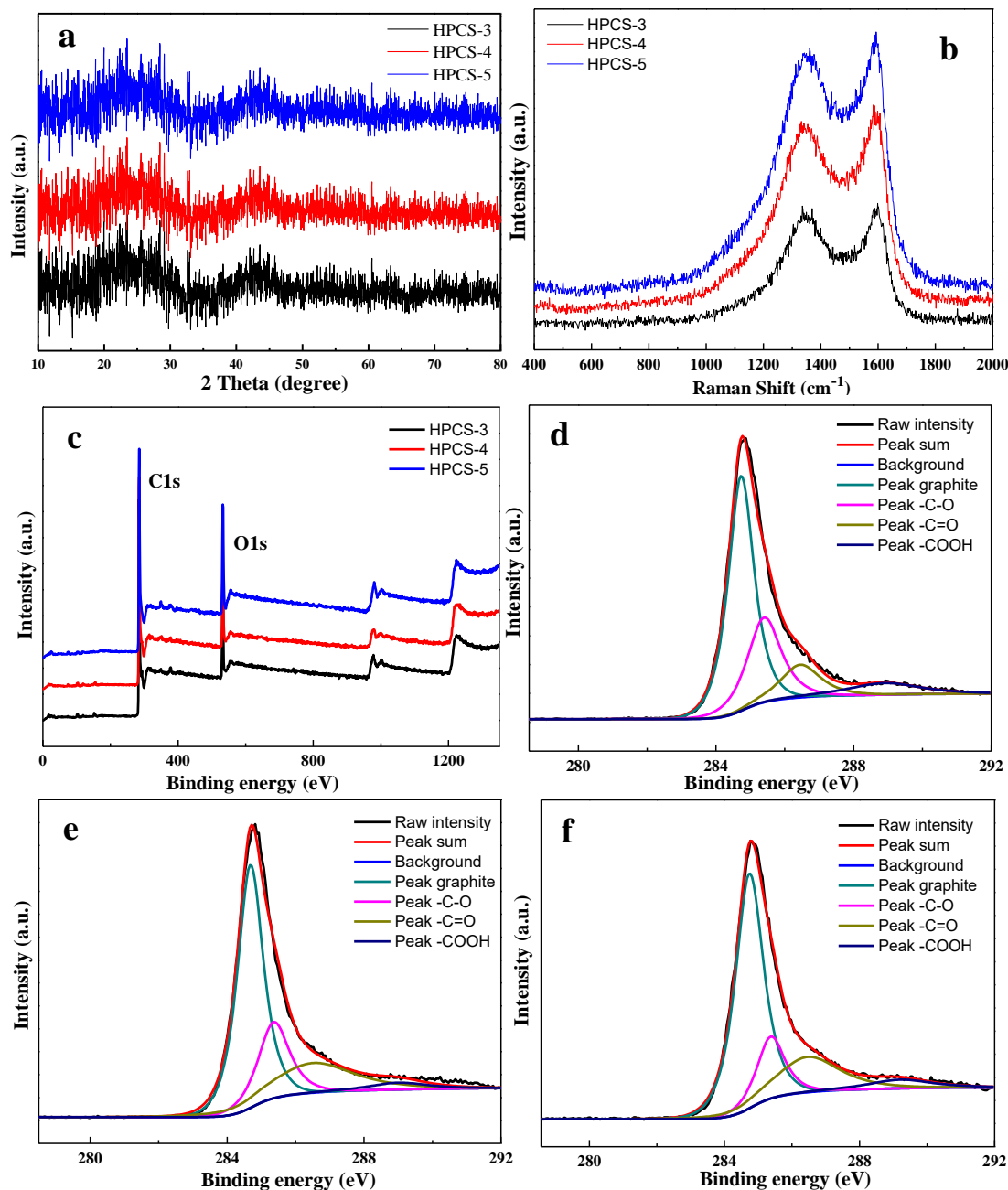


Figure 2. (a) XRD patterns, (b) Raman spectra and (c) XPS spectrum of the HPCS, and high resolution spectrum of C1s for (d) HPCS-3, (e) HPCS-4 and (f) HPCS-5.

The resultant HPCS were further characterized by XRD. As shown in Fig. 2a, HPCS exhibited two weak diffraction peaks at around 24° and 44° . The broad diffraction peak centered at about 24° can

be assigned to the (002) plane of graphite. The peak at around 44° belong to the (101) plane of graphitic layers [30]. Obviously, the intensity of these two peaks reduced with the increase of KOH amount, meaning the graphite layers could be destroyed seriously with more alkaline. Of course, it would create more pores in HPCS due to the etching reaction [33]. Meanwhile, the Raman characterization was adopted in order to further characterize the graphitization of the HPCS. Raman spectra of HPCS (Fig. 2b) displayed two typical peaks, i.e. the D-band located $\sim 1,340\text{ cm}^{-1}$ and a G-band $\sim 1,590\text{ cm}^{-1}$, ascribed to the vibration of disordered carbon atoms with defects and sp^2 -bonded carbon atoms in a two-dimensional hexagonal lattice, which were correspond to the disordered degree and graphitized degree, respectively. The intensity ratios of D band to G band (I_D/I_G) of HPCS-3, HPCS-4 and HPCS-5 were 0.96, 0.93 and 0.94, respectively. The lower I_D/I_G ratio reveals a higher graphitized degree for the HPCS-4 [34]. These results demonstrated that the excessive amount of KOH (1:5) would be harmful to the graphitization of carbon.

The surface property of HPCS was further analyzed by XPS spectra. The fully scanned spectrum of the HPCS exhibited two peaks at 284.4 eV and 532.9 eV (Fig. 2c), which correspond to C1s and O1s, respectively. The fitted high-resolution spectra of C1s for HPCS-3, HPCS-4 and HPCS-5 (Fig. 2d-f) can be deconvoluted into four components with the binding energy at about 284.6, 285.4, 286.5 and 289.0 eV, corresponding to graphite carbon, $-\text{C}-\text{O}-$, $-\text{C}=\text{O}$, and $-\text{COOH}$ groups, respectively [35,36]. For HPCS-3, the mass percentage of graphite carbon, $-\text{C}-\text{O}-$, $-\text{C}=\text{O}$, and $-\text{COOH}$ groups were 54.9, 25.9, 11.7 and 7.5, respectively; 54.9, 20.7, 21.0 and 3.4 % for HPCS-4, respectively; 59.5, 15.6, 20.1 and 4.8% for HPCS-5, respectively. The content of $-\text{C}-\text{O}-$ and $-\text{C}=\text{O}$ groups for HPCS-3, HPCS-4 and HPCS-5 were 37.6, 41.7 and 35.7%, respectively, indicating the maximum amount of oxygen-containing functional groups on the surface of HPCS-4 occurred after activation. These functional groups could improve the wettability of the carbon microspheres and lower the diffusion resistance of electrolytes [37].

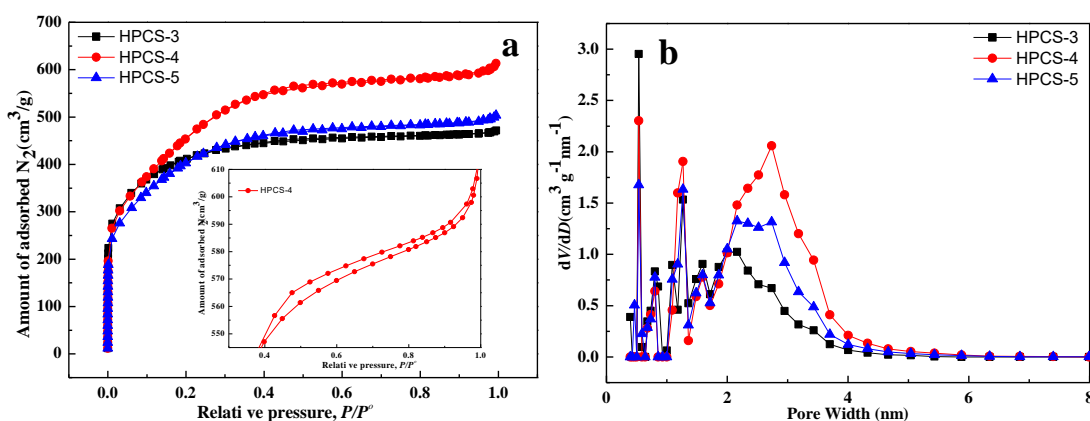


Figure 3. (a) N_2 adsorption/desorption isotherms and (b) the pore size distribution curves of the HPCS. Inset was the N_2 adsorption/desorption isotherms at higher relative pressure (>0.4) for the HPCS-4.

Nitrogen adsorption-desorption isotherms was employed to identify the porosity of the carbon microspheres. According to the IUPAC classification, all the adsorption/desorption isotherms shown in

Fig. 3a should be classified into type I and IV [19]. The amount of adsorbed N₂ rapidly increased even at relative pressure lower than 0.1, confirming the existence of microporous structures in carbon microspheres due to the reaction between carbon and alkaline. At relative pressures larger than 0.1 to 0.3, the amount of adsorbed N₂ rise smoothly. Moreover, a slight hysteresis loop displayed at larger relative pressure of higher than 0.4, confirming the massive mesopores in the carbon microsphere [38], especially for the HPCS-4 (inset of Figure 3a). Furthermore, a slight increase of adsorbed amount observed at the relative pressure close to 1, meaning existence of macropores [30].

Table 1. Parameters of the pore structure of HPCS.

Sample	S_{BET} (m ² /g)	S_{micro} (m ² /g)	S_{mecro} (m ² /g)	V_{tot} (cm ³ /g)	V_{micro} (cm ³ /g)	V_{mecro} (cm ³ /g)	D (nm)
HPCS-3	1419	521	493	0.729	0.297	0.254	2.05
HPCS-4	1652	733	586	0.948	0.416	0.385	2.31
HPCS-5	1440	594	428	0.771	0.318	0.267	2.17

Note: S_{BET} : Specific surface area from multiple BET method.

S_{micro}, V_{micro} : Micropore surface area and micropore volume from t-plot method.

S_{meso}, V_{mecro} : Mecropore surface area and mecropore volume from BJH method.

V_{tot} : Total pore volume at $P/P^0=0.99$.

D : Average pore diameter.

Table 1 compared the porous properties of the HPCS. The surface areas (1652 m²/g) and pore volume (0.948 cm³/g) of HPCS-4 were larger than others, demonstrating that the optimum mass ratio of carbon spheres/KOH is 1:4 in the activation process. In other words, the small amount of KOH is not sufficiently activated carbon spheres, while the excess amount of KOH would lead to collapse of the holes, resulting in decrease of the surface areas and pore volume. Fig. 3b showed the pore size distribution of carbon microspheres by Density Functional Theory (DFT). The pore size ranged from below 2 nm, such as 0.54, 0.84, 1.28 and 1.60 nm (microporous), to ~4 nm (mesoporous). Obviously, massive micropores and mesopores can be formed in carbon microspheres resulting from the reaction between carbon and KOH. It has been reported that a maximum capacitance can be obtained if the pore size in the materials is close to the ion size in the electrolyte [39]. It can be predicted that the smaller pores in carbon microspheres would benefit the formation of electric double-layer and a high capacitance at lower scan rate or current density because the ion size of K⁺ was between 0.36 nm and 0.42 nm [40]. For the micro/mesopores of 1.28 to 4 nm, it would play a great role in diffusion paths formation of electrolyte ion. The small amount of macropores served as ion-buffering reservoirs and reduced the ion transport distance during the processes of electrochemical tests [19]. As a result, the carbon microsphere after KOH activation revealed hierarchical porous structure with micropores, mesopores and macropores, which can minimize the distance of ion diffusion, decrease the ion diffusion resistance and enhance the electric-double-layer capacitance [41-43]. Hence, the hierarchical porosity structure in carbon microsphere after activation would improve the electrochemical performance of EDLCs, especially for HPCS-4 with largest specific surface area, highest mesopore volume and wider pore size distribution.

3.2. Electrochemical performance

The cyclic voltammetry (CV), galvanostatic charge-discharge (GCD), and the electrochemical impedance spectroscopy (EIS) tests were carried out by a two-electrode system at room temperature to investigate the electrochemical performances of the porous carbon microspheres. The CV curves of HPCS were shown in Fig. 4a-c with different scan rates between 5 and 300 mV/s within the operating voltage of 0-1 V in KOH. All of the CV curves displayed good rectangular shape without obvious redox peaks, exhibiting the capacitive features of the electrochemical double layer. CVs of HPCS-3 and HPCS-4 maintained good rectangular-like shape at different scan rates (5-300 mV/s), indicating excellent rate capability and reversibility. As shown in Fig. 4d, the specific capacitance of HPCS-3, HPCS-4 and HPCS-5 were 328.9, 384.5 and 342.4 F/g at 5 mV/s, respectively. The specific capacitance would decline with the increase of scan rate. At 300 mV/s scan rate, the specific capacitance of HPCS-3, HPCS-4 and HPCS-5 decreased to 191.9, 208.3 and 141.6 F/g, respectively. Obviously, the HPCS-4 exhibited the largest specific capacitance from 5 to 300 mV/s, indicating quick ion diffusion into the electrochemically active surface and great capacitive behavior of electrode with fast charge-discharge operations mode [12], consistent with its pore structures.

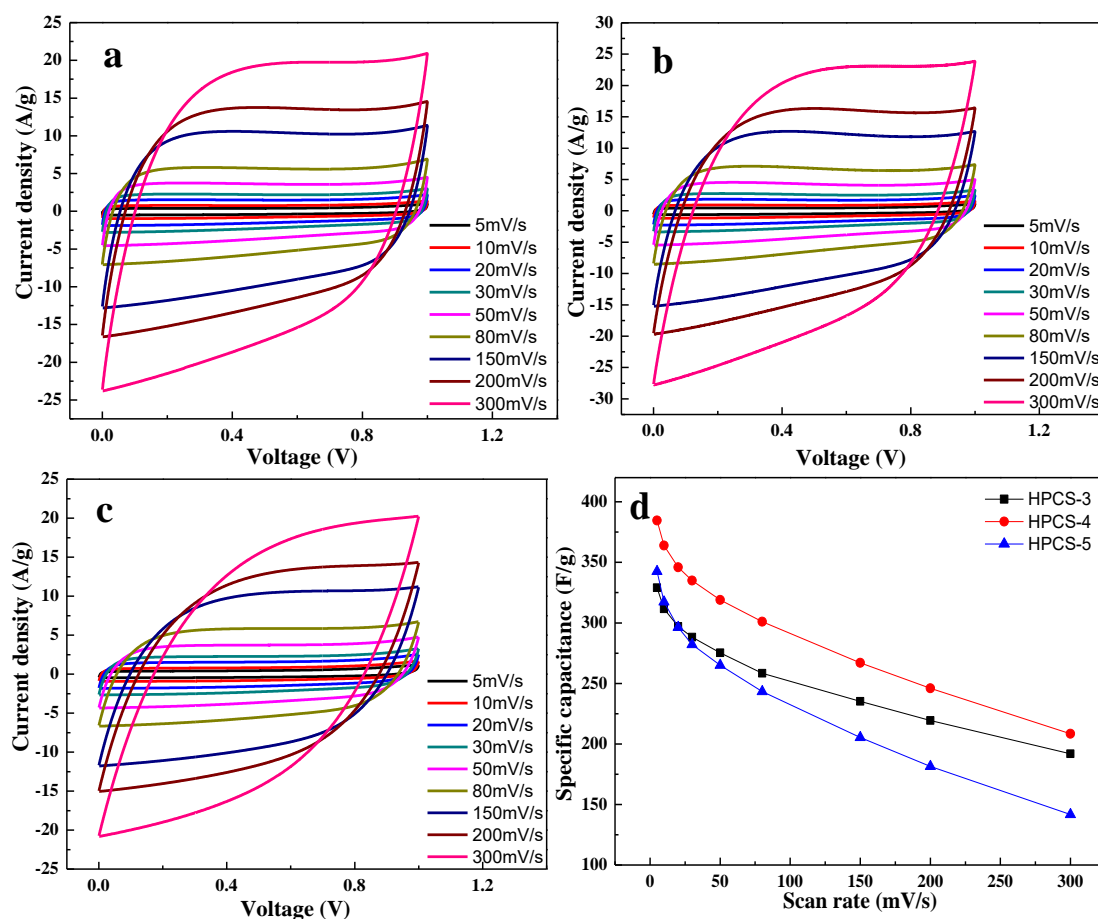


Figure 4. The CV curves of (a) HPCS-3, (b) HPCS-4 and (c) HPCS-5 at the scan rate of 5-300 mV/s within the operating voltage of 0-1 V in 6 M KOH, and (d) specific capacitances of the HPCS at 5-300 mV/s.

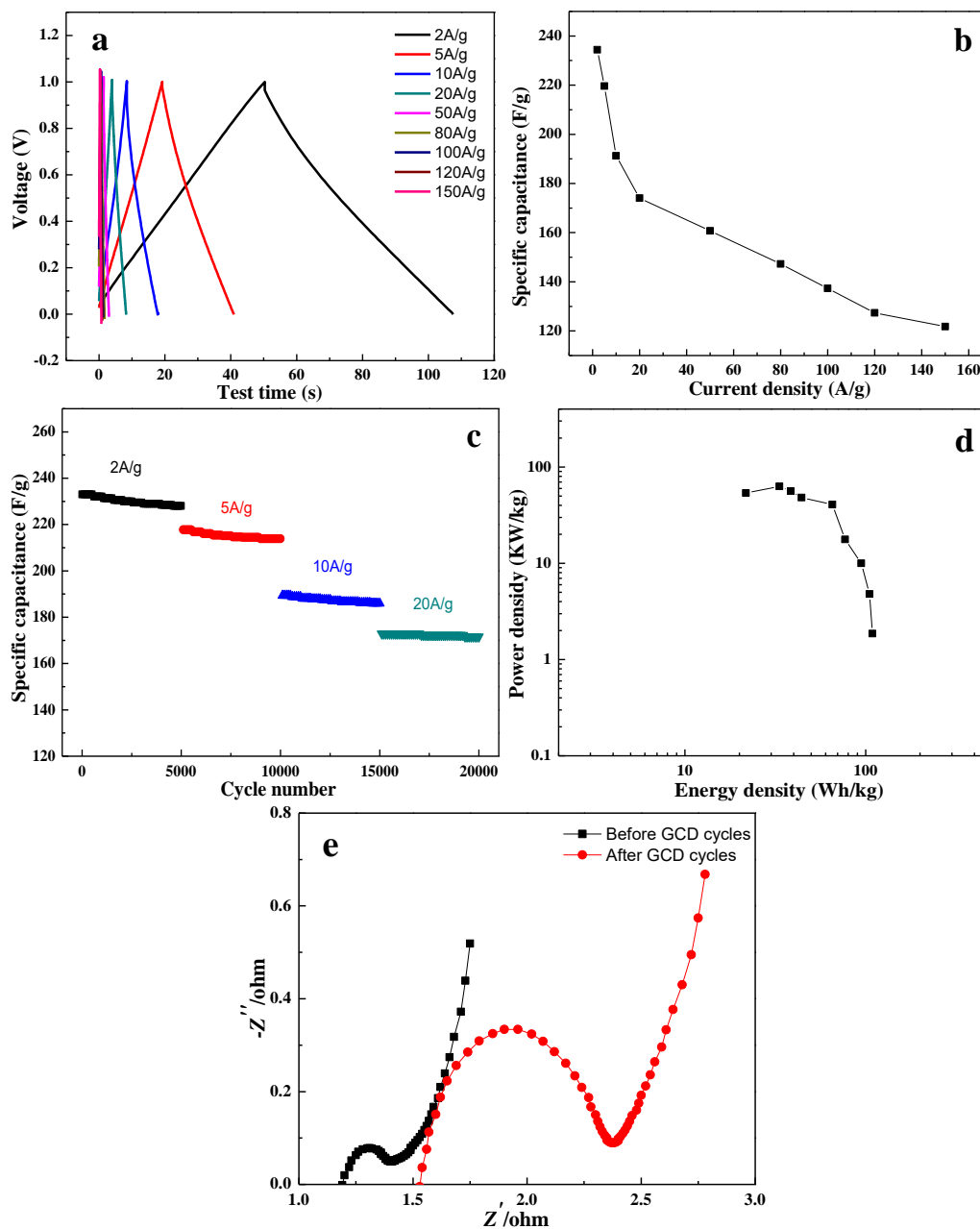


Figure 5. (a) The GCD curves of HPCS-4 at current densities of 2-150 A/g, (b) The specific capacitances of HPCS-4 at current densities of 2-150A/g, (c) The cycling stability of HPCS-4 at 2, 5, 10 and 20 A/g, (d) Ragone plots of HPCS-4 symmetric cell at current densities of 2-150 A/g and (e) Nyquist plots of HPCS-4 measured before and after GCD cycles.

To evaluate further the superior capacitive properties of HPCS-4, the galvanostatic charge-discharge (GCD) of the symmetrical supercapacitors were carried out (Fig. 5a). The charge/discharge curves are almost symmetrical triangular shapes at different current densities between 2 and 150 A/g, indicating the ideal capacitive behavior and stable electrochemical properties. The specific capacitances at different charge/discharge current densities from 2 to 150 A/g was shown in Fig. 5b. The specific capacitance of the HPCS-4 was achieved 234.4 F/g at 2 A/g, and a high rate capacitance

of 137.3 F/g at 100 A/g, corresponding to 58.6% capacitance retention. A high specific capacitance of 121.8 F/g was still achieved even at a higher current density of 150 A/g, corresponding to high capacitance retention of 52.0%. In fact, at lower current density, the higher micropore surface area enhances charge accumulation and the ions have enough time to diffuse into the micropores, therefore the higher specific capacitance can be obtained. However, it was difficult for the ions to diffuse into the internal micropores at relatively high current densities, leading to a drop in the specific capacitance [44]. Although the specific capacitances of HPCS-4 slightly decreased with the increase of current densities, the higher specific capacitance of 137.3 and 121.8 F/g could be obtained even at the current density of 100 and 150 A/g, respectively. The main reason was that the abundant mesopores and small amount of macropores facilitated the transport of ions through these pores to the surface micropores.

The continuously long-term cycling tests of HPCS-4 were carried out over 20000 GCD cycles, namely every 5000 cycles at four different current density (2, 5, 10 and 20 A/g), in order to investigate the rate performance with varied current densities. As shown in Fig. 5c, the specific capacitances of HPCS-4 at different current density of 2, 5, 10 and 20 A/g were 234.4, 219.6, 191.2 and 174.1 F/g, respectively, confirming the excellent rate performances of the carbon microspheres. A high capacity retention of over 97 % with 5000 GCD cycles at each current density revealed the good cycling stability of the carbon microspheres. Therefore, the porous carbon microsphere derived from biomass could be one of the most promising supercapacitor materials.

Meanwhile, the energy density and power density of the supercapacitors assembled with HPCS-4 at various current densities (2-150 A/g) under working voltage of 1.0 V can be calculated from the GCD curves via the equations (3) and (4). The high energy density of 108.9 Wh/kg and power density of 1.86 kW/kg were obtained at 2 A/g current density (Fig. 5d). The energy density will decrease with the current density increasing, but the power density can raise. When the current density up to 50 A/g, the energy density and power density were 65.4 Wh/kg and 40.7 kW/kg, respectively. When the current density was increased to 120 A/g, the energy density could lower to 33.4 Wh/kg, however, the power density raise to 62.9 kW/kg. In addition, it is worth to note that the energy density and power density of supercapacitors using HPCS-4 as the electrodes exhibited much higher value than that of recently reported supercapacitors (Table 2).

Table 2. Comparison of carbon materials for supercapacitor electrodes.

Precursor	Activation agent	Electrolyte	C_s (F/g)	Voltage (V)	E (Wh/kg)@ P (kW/kg)	C_s retention/ Cycle Num.	Ref.
Lignin	ZnCl ₂	6 M KOH	207.5/0.5 A g ⁻¹	1.0	—	89.1%/3000	[6]
Leaves	K ₂ CO ₃ /KOH	6 M KOH	223/0.5 A g ⁻¹	1.0	26.4@18	Almost no decay/2000	[5]
Rice husk	NaOH/KOH	6 M KOH	147/0.1 A g ⁻¹	1.0	5.11@-	85%/10000	[27]
Pine cone	KOH	1 M Na ₂ SO ₄	137/0.1 A g ⁻¹	2.0	19@0.1	100%/10000	[8]
Corn cob residue	KOH	6 M KOH	314/5 mV s ⁻¹ 120/1 A g ⁻¹	1.0	5.3@8.3	100%/100000	[21]
Starch	Ca(CH ₃ COO) ₂	6 M KOH	249.5/10 mV s ⁻¹	1.0	33.89@0.1	99.6%/5000	[38]
Human hair	KOH	6 M KOH	128/80 A g ⁻¹	1.0	—	98%/20000	[43]
White clover	ZnCl ₂	2 M KOH	233.1/1 A g ⁻¹	2.0	30@0.503	100%/5000	[7]
Corn cob	KOH	6 M KOH	384.5/5 mV s ⁻¹ 137.3/100 A g ⁻¹	1.0	33.4@62.9	97%/5000	This work

EIS test was further performed to investigate the charge transport and ion diffusion of the electrode materials. The Nyquist plots of the symmetrical two-electrode cell assembled with HPCS-4 was shown in Fig. 5e before and after the GCD cycles. The nearly vertical lines in low frequency region suggested a short Warburg diffusion region and excellent capacitive property of HPCS-4 [19]. In the high-frequency region, the semicircle corresponded to the interfacial charge transfer resistance (R_{ct}). The internal resistance (R_s) was represented by the intercept points with real axis, including the contact resistance between electrode materials and electrolyte, inherent resistance of materials, and ionic resistance. The R_{ct} values can be obtained from the EIS data fitting via ZSimpWin. The R_{ct} values before and after the GCD cycles were 0.2585 Ω and 0.7558 Ω , respectively, indicating the low resistance and good electrical conductivity of the porous carbon microspheres. The R_s values before and after the GCD cycles were 1.184 Ω and 1.561 Ω , respectively. The slight increase of the R_s value suggested the declined compact degree between the current collector and the electrode material along with the cycles [38]. Hence, the outstanding capacitive performance of HPCS can be ascribed to the combined structure advantages of regular morphology with smooth surface, certain amount of oxygen-containing functional groups, high surface area, hierarchical pores deriving from the KOH activation. Hence, the biomass-corn cob derived carbon microspheres possessed superior supercapacitors performances, which could be an ideal candidate for supercapacitor electrode material.

4. CONCLUSION

One simple and cost-effective hydrothermal carbonization procedure coupling with KOH activation process has been developed to fabricate the carbon microspheres with hierarchical porous structures (HPCS) based on the biomass-corn cob. The HPCS possessed unique regular spherical morphology, oxygen-containing functional groups and developed hierarchical pore structure with micropores, mesopores and macropores. Meanwhile, the obtained HPCS exhibited superior capacitive performance with high specific capacitance, ultra-high rate capability and superior long-term cycle stability through controllable alkaline activation process. Furthermore, the enhancement of power density and energy density of HPCS would satisfy the increasing demands of energy storage devices. Hence, the development of porous carbon microspheres with high capacity derived from crude biomass-corn cob is significantly promising for future design of biomass-derived carbons in specific energy applications. In addition, our work would pave the way for utilization in large-scale and high value added conversion of biomass waste in industry.

ACKNOWLEDGMENTS

This research was supported by Tianjin Research Program of Application Foundation and Advanced Technology (15JCQNJC05700, 15JCQNJC05300 and 14JCYBJC17500), the National Natural Science Foundation of China (No. 21303119), the National Students' Platform for Innovation and Entrepreneurship Training Program (No. 201510058020) and the State Key Laboratory of Inorganic Synthesis and Preparative Chemistry of Jilin University (No. 2017-31).

References

1. Z. Yin, L. Lin, D. Ma, *Catal. Sci. Technol.* 4 (12) (2014) 4116-4128.
2. Z. Yin, H. Zheng, D. Ma, X. Bao, *J. Phys. Chem. C* 113 (3) (2009) 1001-1005.
3. J. Deng, M. Li, Y. Wang, *Green Chem.* 18 (2016) 4824-4854.
4. L. Zhang, Y. Jiang, L. Wang, C. Zhang, S. Liu, *Electrochim. Acta* 196 (2016) 189-196.
5. Y. Li, Y. Pi, L. Lu, S. Xu, T. Ren, *J. Power Sources* 299 (2015) 519-528.
6. L. Li, X. Wang, S. Wang, Z. Cao, Z. Wu, H. Wang, Y. Gao, J. Liu, *Electroanalysis* 28 (2016) 243-248.
7. G. Ma, Z. Zhang, K. Sun, H. Peng, Q. Yang, F. Ran, Z. Lei, *RSC Adv.* 5 (2015) 107707-107715.
8. A. Bello, N. Manyala, F. Barzegar, A. A. Khaleed, D. Y. Momodu, J. K. Dangbegnon, *RSC Adv.* 6 (2016) 1800-1809.
9. Y. K. Lv, L. H. Gan, M. X. Liu, W. Xiong, Z. J. Xu, D. Z. Zhu, D. S. Wright, *J. Power Sources* 209 (2012) 152-157.
10. I. M. D. Salas, Y. N. Sudhakar, M. Selvakumar, *Appl. Surf. Sci.* 296 (2014) 195-203.
11. J. Zhang, J. Zhou, D. Wang, L. Hou, F. Gao, *Electrochim. Acta* 191 (2016) 933-939.
12. W. Lu, M. Liu, L. Miao, D. Zhu, X. Wang, H. Duan, Z. Wang, L. Li, Z. Xu, L. Gan, *Electrochim. Acta* 205 (2016) 132-141.
13. J. Liu, T. Yang, D. Wang, G. Lu, D. Zhao, S. Qiao, *Nat. Commun.* 4 (2013) 2798-2804.
14. A.B. Fuertes, P. Valle-Vigón, M. Sevilla, *Chem. Commun.* 48 (2012) 6124-6126.
15. M. Liu, J. Qian, Y. Zhao, D. Zhu, L. Gan, L. Chen, *J. Mater. Chem. A* 3 (2015) 11517-11526.
16. J. Choma, D. Jamiola, K. Augustynek, M. Marszewski, M. Gao, M. Jaroniec, *J. Mater. Chem.* 22 (2012) 12636-12642.
17. L. Pang, B. Zou, Y. Zou, X. Han, L. Cao, W. Wang, Y. Guo, *Colloid. Surface. A* 504 (2016) 26-33.
18. L. Yao, G. Yang, P. Han, Z. Tang, J. Yang, *J. Power Sources* 315 (2016) 209-217.
19. S. Du, L. Wang, X. Fu, M. Chen, C. Wang, *Bioresour. Technol.* 139 (2013) 406-409.
20. Y. Fan, P. Liu, Z. Yang, T. Jiang, K. Yao, R. Han, X. Huo, Y. Xiong, *Electrochim. Acta* 163 (2015) 140-148.
21. W. Qu, Y. Xu, A. Lu, X. Zhang, W. Li, *Bioresour. Technol.* 189 (2015) 285-291.
22. L. Mao, L. Zhang, N. Gao, A. Li, *Green Chem.* 15 (2013) 727-737.
23. Y. Li, T. Wang, X. Yin, C. Wu, L. Ma, H. Li, Y. Lv, L. Sun, *Renew. Energy* 35 (2010) 583-587.
24. H. Ma, J. Li, W. Liu, M. Miao, B. Cheng, S. Zhu, *Bioresour. Technol.* 190 (2015) 13-20.
25. R. Farma, M. Deraman, A. Awitdrus, I.A. Talib, E. Taer, N.H. Basri, *Bioresour. Technol.* 132 (2013) 254-261.
26. W. T. Huang, H. Zhang, Y. Q. Huang, W. K. Wang, S. C. Wei, *Carbon* 49 (2011) 838-843.
27. E. Y. L. Teo, L. Muniandy, E. Ng, F. Adam, A. R. Mohamed, R. Jose, K. Chong, *Electrochim. Acta* 192 (2016) 110-119.
28. H. Peng, G. Ma, K. Sun, Z. Zhang, Q. Yang, Z. Lei, *Electrochim. Acta* 190 (2016) 862-871.
29. K. Huang, M. Li, Z. Chen, Y. Yao, X. Yang, *Electrochim. Acta* 158 (2015) 306-313.
30. Y. Zhang, M. Jia, H. Gao, J. Yu, L. Wang, Y. Zou, F. Qin, Y. Zhao, *Electrochim. Acta* 184 (2015) 32-39.
31. G.A. Ferrero, M. Sevilla, A.B. Fuertes, *Carbon* 88 (2015) 239-251.
32. C.W. Lee, S. B. Yoon, H. K. Kim, H.C. Youn, J. Han, K. C. Roh, K. B. Kim, *J. Mater. Chem. A* 3 (2015) 2314-2322.
33. J. Wang, S. Kaskel, *J. Mater. Chem.* 22 (2012) 23710-23725.
34. Y. Wang, Y. Song, Y. Wang, X. Chen, Y. Xia, Z. Shao, *J. Mater. Chem. A* 3 (2015) 773-781.
35. X. Fan, C. Yu, Z. Ling, J. Yang, J. Qiu, *ACS Appl. Mater. Interfaces* 5 (2013) 2104-2110.
36. S. Jiang, T. Shi, X. Zhan, H. Long, S. Xi, H. Hu, Z. Tang, *J. Power Sources* 272 (2014) 16-23.
37. V. Sahu, S. Shekhar, R. K. Singh, G. Sharma, *ACS Appl. Mater. Interfaces* 7 (2015) 3110-3116.

38. Y. Zhang, M. Jia, J. Yu, J. Fan, L. Wang, Y. Zou, Y. Zhao, *J Solid State Electrochem* 20 (2016) 733-741.
39. C. Largeot, C. Portet, J. Chmiola, P.L. Taberna, Y. Gogotsi, P. Simon, *J. Am. Chem. Soc.* 130 (2008) 2730-2731.
40. L. Eliad, G. Salitra, A. Soffer, D. Aurbach, *J. Phys. Chem. B* 105 (2001) 6880-6887.
41. Y. F. Zhao, W. Ran, J. He, Y. F. Song, C. M. Zhang, D. B. Xiong, F. Gao, J. Wu, Y. Xia, *ACS Appl. Mater. Interfaces* 7 (2015) 1132-1139.
42. C. Zhang, W. Lv, Y. Tao, Q.H. Yang, *Energy Environ. Sci.* 8 (2015) 1390-1403.
43. W. J. Qian, F. X. Sun, Y. H. Xu, L. H. Qiu, C. H. Liu, S. D. Wang, F. Yan, *Energy Environ. Sci.* 7 (2014) 379-386.
44. Z. Qiao, M. Chen, C. Wang, Y. Yuan, *Bioresour. Technol.* 163 (2014) 386-389.

© 2017 The Authors. Published by ESG (www.electrochemsci.org). This article is an open access article distributed under the terms and conditions of the Creative Commons Attribution license (<http://creativecommons.org/licenses/by/4.0/>).